

**International Journal of Vehicle Performance**

ISSN online: 1745-3208 - ISSN print: 1745-3194

<https://www.inderscience.com/ijvp>

---

**Modelling of detailed vehicle dynamics and quantitative impact of electric motor placement on regenerative braking**

Shantanu Pardhi, Ajinkya Deshmukh, Hugo Ajrouche

**DOI:** [10.1504/IJVP.2022.10046859](https://doi.org/10.1504/IJVP.2022.10046859)

**Article History:**

Received:	04 May 2021
Accepted:	13 December 2021
Published online:	04 January 2023

---

## **Modelling of detailed vehicle dynamics and quantitative impact of electric motor placement on regenerative braking**

---

Shantanu Pardhi\*, Ajinkya Deshmukh  
and Hugo Ajrouche

Capgemini Engineering,  
Research & Innovation France,  
147-151 Quai du Président Roosevelt,  
92130, Issy-les-Moulineaux, France  
Email: shantanu.pardhi@vub.be  
Email: ajinkya.deshmukh@altran.com  
Email: hugo.ajrouche@altran.com

\*Corresponding author

**Abstract:** Using forward type vehicle simulation, this paper aims at comparing the potential and limitations of front wheel drive and rear wheel drive electric motor placements for regenerative braking under extreme driving situations. First, the considered dynamic/data-driven modelling approach for the complete traction chain with attention to the effects of detailed vehicle dynamics has been implemented in MATLAB Simulink. Simple parallel regenerative braking technique and recuperation favouring brake distribution strategies have been employed on a performance electric car example considering front and rear wheel propulsion cases. Powertrain behaviour in a dynamic driving scenario has been investigated to understand how the two cases with their corresponding recuperation favouring braking strategies perform under elevated transient vehicle dynamics. Finally, the impact of normal load transfer, tyre slip and wheel adhesion limits on regenerative braking has been quantitatively compared for the complete range of brake pedal demands using high-speed braking tests while avoiding wheel lock-up.

**Keywords:** regenerative braking; electric motor axle placement; vehicle dynamics; wheel slip; normal load transfer; powertrain modelling; brake bias strategy; FWD; front wheel drive; RWD; rear wheel drive; simulation.

**Reference** to this paper should be made as follows: Pardhi, S., Deshmukh, A. and Ajrouche, H. (2023) 'Modelling of detailed vehicle dynamics and quantitative impact of electric motor placement on regenerative braking', *Int. J. Vehicle Performance*, Vol. 9, No. 1, pp.16–40.

**Biographical notes:** Shantanu Pardhi is a powertrain engineer specialising in hybridisation, electrification and combustion engine development. With a key focus on engineering simulation, control system development and dynamic modelling of powertrain behaviour, Shantanu pursues internal research projects as well as external industrial client requirements. Along with his experience, a Masters in Automotive Engineering with specialisation in energy management

and a bachelors in mechanical engineering gives him a solid base to tackle engineering challenges.

Ajinkya Deshmukh received his PhD in Mechatronics systems and devices. He has a background in electromagnetic actuation and control systems. He is currently involved in the technical management of R&I projects relating to hybrid and electric powertrains. His research interests include development of energy management system for hybrid vehicles, energy and size optimisation and design of control strategies.

Hugo Ajrouche has a Master Degree in Laser Optical and Nanotechnology Engineering at the Universite de Bordeaux, where he worked on a thesis entitled: "Transport phenomena at small scales of time and space". He has a PhD Degree from INSA Rouen Normandie where he worked on a thesis entitled: "Thermography and Multi-species Concentration Measurement by Spontaneous Raman Scattering for Turbulent Combustion". Then, he became a post-doc researcher in the experimental analysis of combustion at Polytech Orleans where he conducts research dealing with optical diagnostics for combustion as LIF, X-ray diagnostic, Schlieren, Diffused Back-illumination in a new one shot engine. Currently, he is Project Leader at Capgemini Engineering where he managed R&I project related hybrid powertrain modelling and simulation.

---

## 1 Introduction

To reduce the impact of increasing local and global  $CO_2$  emissions on the environment, the modern-day automotive industry is shifting towards electrified powertrains. Following this path, various agreements have been made in European and global markets on future sustainable mobility (EU, 2016; IEA, 2018; Niestadt and Bjørnåvold, 2019). One of the important features that maximise the overall cycle efficiency of an electrified powertrain is its ability to recuperate a portion of kinetic energy from the moving vehicle during braking through electric machine operation in generator mode which would otherwise be lost as heat in friction brakes (Clegg, 1996). This recovered energy can then be used as the primary or the supporting means of tractive power in motor mode thereby consuming less of the original available source and improving powertrain efficiency (Qiu et al., 2018). Other applications of the recuperated energy could also include its usage in intelligent energy management for hybrid vehicles by assisting the main prime mover in its efficient functioning and in running auxiliary loads (Ahmadi et al., 2018; Hofman et al., 2006).

Various papers have been published on calculating, analysing and optimising electric powertrain energy efficiency (Jiang et al., 2018; He et al., 2014; Du et al., 2017; Ruan et al., 2014). An effective braking strategy is essential in optimising the energy recuperation while maintaining vehicle stability (Ehsani et al., 2018; Heno-Muñoz et al., 2020). The impact of vehicle dynamics also plays a key role in maximising the possible recoverable braking energy (Crolla and Cao, 2012). Kumar and Subramanian (2015) have previously presented a regenerative braking strategy for series hybrid electric vehicles, which focuses on modifying conventional braking to achieve higher energy recovery. The combined braking strategy presented promising results by recuperating twice the braking energy as that from conventional parallel braking. Sangtarash et al. (2008) has shown the comparison

of series and parallel regenerative braking strategies towards higher energy recuperation. The simulations were carried out on a hybrid electric bus and it has been concluded that compared to the conventional bus, series and parallel braking strategies regenerate 33.5% and 19.6% energy respectively.

Xiao *et al.* (2017) has proposed a regenerative braking technique based on the ideal front-rear brake force distribution curve and operational limits of the electrical powertrain. A fuzzy logic controller has been used to improve braking system response and comparison with serial and eco braking strategies through simulation has presented favourable improvements. Itani *et al.* (2016) has compared sliding mode wheel slip controller and ECE R13H constraints derived braking methods for maximising regenerative energy recovery of a front-wheel driven vehicle and have demonstrated simulation results for low-speed extreme braking under changing road friction levels. Xu *et al.* (2019) implemented a model predictive control based holistic regenerative braking strategy on four in-wheel motors equipped electric vehicle and has demonstrated higher efficiency over rule-based strategy for dry, wet and snow road conditions through simulations. Furthermore, Le Solliec *et al.* (2013) has also studied regenerative braking under changing road adhesion levels considering longitudinal slip control. Henao-Muñoz *et al.* (2020) has discussed possible efficiency maximising regenerative braking strategies for Formula SAE electric race car running on a highly transient racetrack drive cycle. The strategy aims at maximising the recovery of braking energy by placing as much braking force as possible on the powered axle while avoiding the locking of the front and rear wheels. Results have been compared with friction only, fixed distribution and ideal wheel adhesion based variable brake force distribution strategies and it has been shown that the proposed strategy is able to recover energy with a percentage difference of 31.2% as compared to the ideal brake distribution and thereby also able to reduce the mass of the electric vehicle by 3.4% increasing its performance. In addition, specific braking strategies aimed at recovering maximum kinetic energy for increasing electric vehicle autonomy have also been evaluated in several other papers (Guo *et al.*, 2009; Xu *et al.*, 2011; Wang and Zhuo, 2008; Zhang *et al.*, 2012; Guo *et al.*, 2021).

Most of the previous work has mainly focused on regenerative braking strategies for front or rear wheel electric, hybrid drives and the use of various energy management techniques in optimising power flow. However, a comparison of the effect of detailed vehicle dynamics on the regenerative braking ability of front and rear wheel drive electric powertrains has not been seen especially under non-ideal extreme driving situations. To fill in this research gap, the current work aims at comparing the effect of front and rear wheel drive electric axle placement towards maximising regenerative braking efficiency for the complete range of possible brake pedal demands including those seen in intense braking. During high acceleration, front wheel drive (FWD) placement tends to be traditionally weaker in terms of maintaining wheel adhesion when compared to rear wheel drive (RWD) due to lower peak road force transmission capability. However, this effect of normal load transfer between the front and rear and the corresponding change in wheel adhesion limits also give the front axle greater force transmission ability during braking. The main originality of the current work will be, to quantitatively analyse the effect of detailed vehicle dynamics including front-rear normal load transfer and wheel slip on the losses and limitations of possible recuperable braking energy. The impact of these aspects is more pronounced under highly transients conditions and will thus be studied for dynamic driving and extreme deceleration scenarios inspired from Oleksowicz *et al.* (2013).

The paper is divided into several sections. Section 1, explains the modelling approach that has been used to simulate the behaviour of different aspects of vehicle dynamics and traction chain. A high-performance vehicle use case capable surpassing the possible limits of wheel adhesion during intense acceleration and deceleration has been selected for this analysis as presented in Section 2. Section 3, explains the focused brake bias distribution concepts for the two architectures and regenerative braking strategy adopted in this paper. Section 4, provides the results and analysis of dynamic driving and high-speed braking tests. At last, Section 5, gives conclusion and future perspectives of the presented work.

## 2 Modelling methodology

### 2.1 Vehicle dynamics

In this section, a dynamic/data-driven vehicle modelling approach has been presented to simulate detailed longitudinal vehicle dynamics affecting the powertrain behaviour under intense driving conditions. This allows for the analysis of individual component states (front wheels, rear wheels, electric drive, vehicle body) and their impact on the behaviour of the complete traction chain (James et al., 2020). The modular and generic nature of this approach also supports the implementation of any type of vehicle and powertrain architecture providing the possibility to define electric drive placement on the front axle, rear axle or even on all four wheels. The proposed methodology has been modelled using MATLAB/Simulink software.

The approach consists of a complete vehicle dynamics representation, including two separate wheel models representing the front and rear wheels with their respective rotational inertias and friction-slip characteristics (two-wheel approach) (see Figure 1). A vehicle model is used to simulate the effect of tractive and braking forces being transmitted by the front and rear wheels on the actual vehicle speed. A front-rear normal load transfer representation has also been implemented to take into account the varying normal load and changing friction-slip behaviour of the front and rear wheels. An in house driver block provides the accelerator and brake pedal inputs to follow the desired vehicle speed. Two identical mechanical brake models have been installed to represent the front and rear parts of the braking system, respectively. The powertrain consists of an electric traction chain with a simplified models of the transmission, electric machine (EM) and battery. To regulate such forward type vehicle model, dedicated control has been defined for allowing the powertrain to generate the required torque and power demand while still respecting component safety limits. The modelling technique used to define the various components has been briefly described below while the interaction of component blocks and subsystems can be referred to in Pardhi et al. (2021).

#### 2.1.1 Vehicle

The vehicle model calculates the effect of tractive and braking force on the vehicle speed. The total force to the road  $F_{trnsf}$  is found from the sum of front and rear wheel transmitted forces (equation (1)).

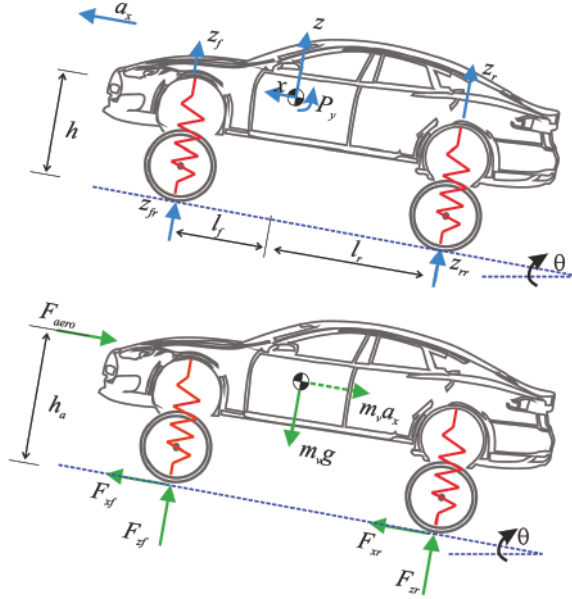
$$F_{trnsf} = F_{xf} + F_{xr} \quad (1)$$

To determine the actual vehicle speed, the impact of aerodynamic drag, rolling resistance, longitudinal inertia and the road inclination are considered (equation (2)).

$$\frac{dV_v}{dt} = \frac{F_{trnsf} - (\frac{1}{2}\rho_a A_v C_d V_v^2 + C_{rr} m_v g \cos\theta + m_v g \sin\theta)}{m_v} \quad (2)$$

where  $A_v$  is the vehicle frontal area,  $C_d$  is the aerodynamic drag coefficient,  $\rho_a$  is the ambient air density,  $C_{rr}$  is the wheel rolling resistance coefficient,  $m_v$  is the vehicle mass and  $\theta$  is the road inclination angle in degrees (positive for ascending and negative for descending gradient) (Guzzella and Sciarretta, 2013; Kuhlwein, 2016).

**Figure 1** Trivial suspension for load transfer model (see online version for colours)



### 2.1.2 Load transfer

Normal load transfer between the front and rear wheels (axes) due to vehicle acceleration and deceleration has been implemented using a quasi-steady state approach. The model is able to calculate the instantaneous vertical load on the front and rear axle by taking into account the actual vehicle speed, acceleration, overall applied wheel force, aerodynamic resistance and road gradient (Jacobson, 2016). Figure 1, represents this trivial suspension load transfer model.

When the vehicle is stationary, only the effect of centre of gravity and road inclination  $\theta$  act on the weight distribution between the front  $F_{zfo}$  and the rear  $F_{zro}$  (equation (3)).

$$F_{zfo} = \frac{m_v g (l_r \cos(\theta) + h \sin(\theta))}{l_f + l_r} \quad F_{zro} = \frac{m_v g (l_f \cos(\theta) - h \sin(\theta))}{l_f + l_r} \quad (3)$$

As the vehicle moves, the deformation of front and rear suspension generates reaction forces that vary the normal load distribution between the front and rear wheels  $F_{zf}$ ,  $F_{zr}$  (see equation (4)). Here,  $z_f$  and  $z_r$  are the vertical movements of the front and rear suspension top mounts while  $z_{fr}$  and  $z_{rr}$  are the wheel-road contact point vertical movements which could be used to take into account road unevenness with positive movement in the upward and negative in the downward direction (neglecting the loss of wheel-road contact) (Shakouri et al., 2010). Here,  $c_f$  and  $c_r$  are the overall stiffnesses of front and rear parts of the suspension respectively.

$$F_{zf} = F_{zfo} + c_f(z_{fr} - z_f) \quad F_{zr} = F_{zfo} + c_r(z_{rr} - z_r) \quad (4)$$

Equation (5) represents the effect of pitch  $z$  and heave  $P_y$  vehicle body movements on the overall suspension deformation  $z_f$ ,  $z_r$ .

$$z_f = z - l_f P_y \quad z_r = z + l_r P_y \quad (5)$$

These movements are affected by the amount of applied tractive and braking force  $F_{trnsf}$ , aerodynamic drag force  $F_{aero}$ , height of the aerodynamic centre  $h_a$  and the horizontal  $l_f$ ,  $l_r$  and vertical position  $h$  of the centre of gravity as considered in equations (6) and (7), respectively.

$$z = -\frac{(c_f l_f - c_r l_r)}{c_f c_r (l_f + l_r)^2} (F_{trnsf} h + F_{aero} (h_a - h)) \quad (6)$$

$$P_y = -\frac{(c_f + c_r)}{c_f c_r (l_f + l_r)^2} (F_{trnsf} h + F_{aero} (h_a - h)) \quad (7)$$

The normal loads on the front and rear wheels  $F_{zf}$ ,  $F_{zr}$  are used in their respective wheel models to determine the available grip, force-slip relationship and the amount of force that the wheels can transmit without entering the non-linear slipping zone (lock-up or spin up)(see Figure 2). Being quasi-static in nature, this method does not consider the damping dynamics of the dampers, tyres, bushings and linkages. Effect of longitudinal force transfer in the linkages and the separate impact wheel torque from the brakes (unsprung) and the powertrain (sprung) sources is also not modelled here.

### 2.1.3 Wheel

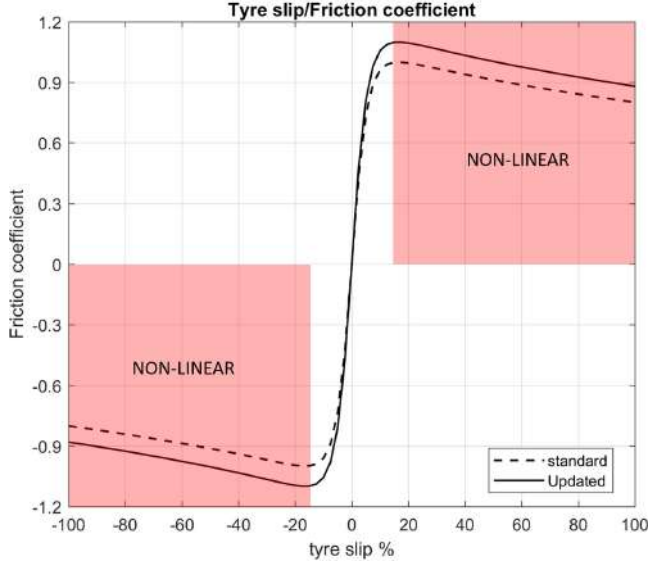
The wheel model calculates the amount of force that the front or rear tyres transmit to the road based on the vertical force on the wheel  $m_v g$  and the instantaneous friction coefficient  $\mu$  (equation (8)). This force being transmitted between the wheel and the road is generated on account of slipping of the wheel (Pacejka, 2000; Rabhi et al., 2007).

$$F_x = m_v g \mu \quad (8)$$

To define the relationship between varying friction coefficient  $\mu$  and generated wheel slip  $k$ , the empirical magic tyre formula has been implemented (see Figure 2) (equation (9)).

$$\mu = D \sin(C * \arctan(Bk - E(10k - \arctan(Bk)))) \quad (9)$$

**Figure 2** Representation of Magic formula: slip - friction coefficient (force) relationship (see online version for colours)



The longitudinal wheel slip  $k$  is the ratio of the difference between actual wheel speed  $\omega_{wrl}$  (with slip) and ideal wheel speed  $\omega_{widl}$  (without slip) to the ideal wheel speed (equation (10)) (Singh and Taheri, 2014). To avoid slip calculation errors at near-zero ideal wheel speed (vehicle speed), the second mentioned formula is used.

$$k \equiv \begin{cases} \frac{\omega_{wrl} - \omega_{widl}}{\omega_{widl}} & \text{if } \omega_{wrl} > 0 \\ \text{OR} \\ \frac{2 * (\omega_{wrl} - \omega_{widl})}{(\omega_{th} + \frac{(\omega_{widl})^2}{\omega_{th}})} & \text{if } \omega_{wrl} \simeq 0 \end{cases} \quad (10)$$

For calculating the actual wheel speed  $\omega_{wrl}$ , balance of various torques at the wheel is considered (equation (12)).

$$\omega_{widl} = \frac{V_v}{r_w} \quad (11)$$

$$\omega_{wrl} = \frac{1}{J_{whl}} \int (T_{pwt} - T_{brk} - T_x) dt \quad (12)$$

where  $T_{pwt}$  is the powertrain torque,  $T_{brk}$  is the mechanical brake torque,  $T_x$  is the actual torque being transmitted to road (equation (8)) and  $J_{whl}$  is the wheel rotational inertia. The ideal wheel speed  $\omega_{widl}$  (for zero slip) is obtained from the actual vehicle speed  $V_v$  and wheel radius  $r_w$ .

## 2.2 Transmission

The torque transmitted between the powertrain and the wheels can be described as equation (13)

$$T_{pwt} = (T_{em} \times I_G - J_{trns} \frac{d\omega_{trns}}{dt}) \eta_{trns} \quad (13)$$

Where,  $I_G$  is the selected gear ratio,  $J_{trns}$  is the transmission rotational inertia at its input,  $\eta_{trns}$  is the transmission efficiency and  $T_{em}$  is the output torque of the electric machine. The transmission speed  $\omega_{trns}$  is then determined from the actual wheel speed  $\omega_{wrl}$  using equation (14).

$$\omega_{trns} = \omega_{wrl} \times I_G \quad (14)$$

### 2.3 Electric machine

With focus on analysing the impact of detailed vehicle dynamics on regenerative braking, a simplified representation of the electric machine (EM) has been used. The EM output torque  $T_{em}$  is calculated from equation (15).

$$T_{em} = T_{em_m} - T_f - J_{em} \frac{d\omega_m}{dt} \quad (15)$$

where  $J_{em}$  is the EM armature rotational inertia,  $\omega_m$  is the EM angular speed ( $=\omega_{trns}$ ) and  $T_{em_m}$ ,  $T_f$  and  $T_{em}$  are the EM electromagnetic, frictional and output torques, respectively. In addition, the EM electrical power for regeneration and traction  $P_{elec}$  is calculated using map based EM efficiency  $\eta_{em}$ , torque  $T_{em_m}$  and speed  $\omega_m$  in equations (16) and (17), respectively.

$$P_{elec} = T_{em_m} \omega_m \eta_{em} \quad (16)$$

$$P_{elec} = \frac{T_{em_m} \omega_m}{\eta_{em}} \quad (17)$$

### 2.4 Battery

A basic equivalent circuit battery model has been implemented for further simplification of the electric powertrain based on the electric power and state of charge (*SoC*). The power delivered to/taken from the battery  $P_{batt}$  is impacted by the power electronics (PE) efficiency  $\eta_{PE}$  as shown in equations (18) and (19) respectively.

$$P_{batt} = P_{elec} \eta_{PE} \quad (18)$$

$$P_{batt} = \frac{P_{elec}}{\eta_{PE}} \quad (19)$$

Moreover, the power from the battery  $P_{batt}$  and its ohmic losses give the actual battery power during discharging and charging in equation (20) and (21) respectively (Pardhi, 2020).

$$V_{oc} I_{batt} = P_{batt} + (I_{batt})^2 R \quad (20)$$

$$V_{oc} I_{batt} = P_{batt} - (I_{batt})^2 R \quad (21)$$

where  $V_{oc}$  is the battery open circuit voltage,  $I_{batt}$  is the battery current and  $R$  is the equivalent resistance of all cells combined. The State of Charge *SoC* is determined from maximum charge capacity  $C_{battmax}$  and instantaneous capacity of the battery  $C_{batt}$  which depends on the discharge/charge current  $I_{batt}$  (equation (22)).

$$C_{batt}(t) = C_{batt}(0) - \int_0^t I_{batt} dt \quad SoC(t) = \frac{C_{batt}(t)}{C_{battmax}} \quad (22)$$

### 3 Vehicle specifications

To study the effect of increased wheel slip and normal load transfer on regenerative braking under extreme driving conditions, Tesla model S 2012 RWD was selected as the use case on accounts of its almost equal front-rear static weight distribution and enough powertrain potential to exceed the wheel adhesion limits (Tesla, 2012; D.Sherman, 2014; Bruen and Marco, 2016; Hust, 2018). For simplifying the analysis of detailed vehicle dynamics impact on energy recuperation under heavy braking, the EM and power electronics efficiencies were kept constant with values adjusted to match the overall powertrain simulation efficiency and range results claimed for the standard vehicle (see Table 1).

**Table 1** Vehicle specifications

<i>Vehicle name</i>	<i>Tesla model S signature performance (2012)</i>
Vehicle weight with one driver [kg]	2181
Vehicle aero drag coefficient	0.24
Vehicle frontal area [ $m^2$ ]	2.341
Powertrain type	RWD, full electric
Wheel radius [m]	0.3515
Tyre rolling resistance coefficient	0.01 (assumed)
Tyre peak friction coefficient	1.1 (calibrated)
Wheel rotational inertia [kgm <sup>2</sup> ]	1 (assumed)
Centre of gravity position [m] (behind front axle/ before rear axle/ ground vertical)	1.5392 / 1.4208 / 0.4572
Wheel base [m]	2.96
Static weight distribution	48:52
Maximum total braking torque to wheels [Nm]	10000 (assumed)
Gearbox type	Single ratio transaxle
Gear ratio (combined with final driver)	9.73:1
Gearbox rotational inertia [kgm <sup>2</sup> ]	0.3 (assumed)
Total transmission efficiency [%]	95 (assumed)
Electric machine EM type	3-phase,4-pole, AC induction
Electric machine average efficiency [%]	91 (assumed)
Inverter and power electronics average efficiency [%]	95 (assumed)
Peak motor torque [Nm]	600 Nm (0–5100 rpm)
Peak motor power [W]	310 kW (5000–8600 rpm)
Peak motor speed [RPM]	16000 rpm
EM rotational inertia [kgm <sup>2</sup> ]	0.025 (assumed)
Battery type	Liquid-cooled, lithium-ion, 85 kWh
Simplified battery architecture	96 series ; 74 parallel
Cell	Panasonic NCR18650B
Cell charge capacity [Ah]	3.1
Cell resistance [ohm]	0.0481
Cell nominal open circuit voltage [V]	3.7
Cell cut-off voltage (charge/discharge) [V]	4.2/2.5
Maximum cell current [A]	15.5

For assuring that the tyre characteristics from the simulation closely resemble those seen on the real world application, the magnitude of the tyre slip-force relationship was adapted

to match the 0–100 km/h claimed acceleration performance of the selected vehicle of 4.4 s (as shown in Figure 2). For this, wheel spin up due to excessive powertrain torque output was avoided by simply saturating the driver accelerator pedal demand to 94% above which the powered wheels would lose traction, spin up and generate reduced performance. With this method, a 0–100 km/h time of 4.29s was achieved and later with the application of precisely tuned simplified traction control intervention (TC) the best possible time of 4.39s was found (Table 2).

**Table 2** Traction control calibration

System delay margin [ms]	10
System trigger slip point [%]	30
Torque cut on trigger [%]	12

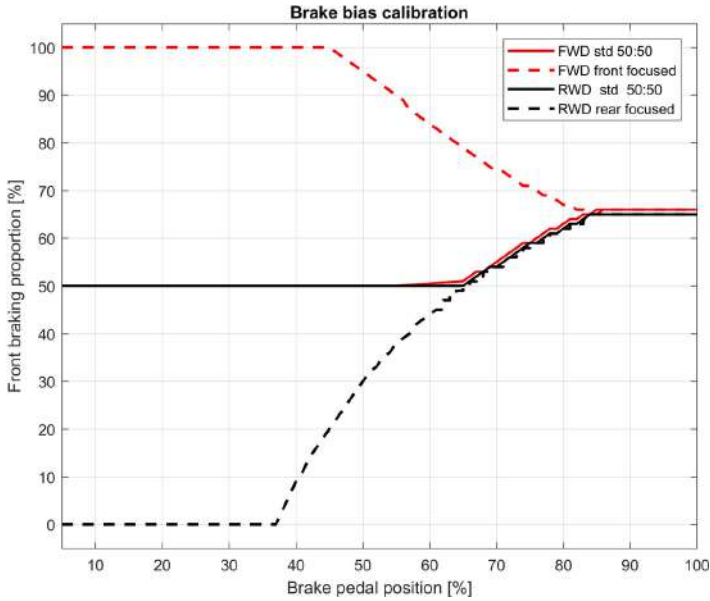
## 4 Control

### 4.1 Brake bias distribution

In this section, simple static feed-forward front-rear brake distribution strategies has been considered depending on the driver's brake pedal application as shown in Figure 3. The focus has been on maximising the use of changing grip levels of the front and rear wheels due to vehicle dynamics for achieving the best possible braking performance while still avoiding unsafe driving situations such as rear wheel lock-up (Jacobson, 2016). For calibrating these fixed strategies, we start from 50/50 front-rear brake distribution, which is generally used in conventional vehicles for normal driving to minimise wear and tear. With increasing brake pedal application, the distribution of the braking effort on recurring 200-0 km/h braking tests is initially maintained equal between the front and rear until possible. As braking intensity is further increased, so does the deceleration and the normal load transfer from the rear to the front of the vehicle. With this decrease in vertical load on the rear wheels their ability to transmit braking force decreases while the opposite is seen for the front wheels. Above 65% brake pedal application, with a further increase in applied braking torque, the rear wheels start to lock-up (stop rotating) generating reduced overall deceleration and making the vehicle laterally unstable (Jacobson, 2016). To avoid this, the proportion of the total braking torque to the rear wheels is simultaneously decreased and transferred to the front where the adhesion limits are rising (change in brake bias). This procedure is repeated for recurring high speed braking tests with increasing brake pedal application requiring a gradual change in brake bias to avoid rear wheel lock-up Figure 3. After an increase in brake pedal input above 84%, both front and rear wheels begin to lock-up for all cases, meaning the ability of the complete vehicle to generate higher deceleration has been reached and above this, the vehicle will have decreased braking performance due to transmission of lower overall braking force to the road (refer to Figure 2).

The slight difference between calibrated standard brake bias strategies for the FWD and RWD cases as seen in Figure 3 is due to the higher sensitivity of FWD case to rear wheel lock-up as compared to RWD case on accounts of reduced overall rear axle rotational inertia (absence of rear powertrain).

**Figure 3** Simple feed-forward brake distribution strategies for favouring regenerative braking (see online version for colours)



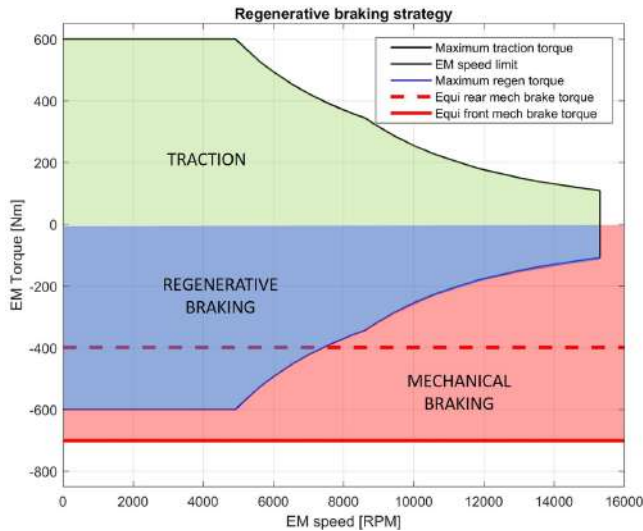
To maximise the regenerative braking ability of the electrical powertrain, brake bias distribution strategies specifically favouring braking with the powered axle are now calibrated for FWD and RWD cases and will be considered for further analysis due to their proven improvements (Henaio-Muñoz et al., 2020) Figure 3. In the case of the FWD front regeneration focused strategy (red - -), the braking force is transmitted only by the front wheels for as long as possible to maximise regeneration potential within the vehicle safety limits. Once the front wheel adhesion limit is reached, the overall deceleration can then further be increased by introducing braking to the rear wheels through a reduction in the proportion of the brake bias going to the front and transferring it to the rear (seen after 45%) as shown in Figure 3. For the RWD rear focused case (black - -), the rear wheels are used for as long as possible while front-wheel braking is introduced only when the limit of adhesion of the rear wheels is reached to avoid their lock-up. Rear wheel lock-up for the RWD case starts to occur earlier as compared to FWD due to the different adhesion limits on account of normal load transfer during braking.

#### 4.2 Regenerative braking

A simple regenerative braking strategy based on completely replacing mechanical braking torque of the powered axle with electro-mechanical braking torque from the EM has been considered in this work. If the braking torque demand for that axle surpasses the possible torque, power or speed limits of the electric machine (EM), mechanical brakes would be used in tandem to support the braking of that axle along with the EM (see Figure 4). It can be seen in Figure 4 that for our specific vehicle use case, the equivalent of maximum wheel braking torque at the level of EM output (including transmission losses) in the case of the front wheels is much higher than the EM peak torque curve for all operational speeds (red - derived during brake bias calibration procedure). On the other hand, for the rear wheels,

the EM is capable of completely replacing the mechanical brakes at lower speeds (below 7500 RPM) (red - -).

**Figure 4** Simple parallel regenerative braking strategy (see online version for colours)



## 5 Results and discussion

### 5.1 Dynamic driving

For comparing the transient behaviour of vehicle dynamics and traction chain for the two distinct regeneration focused cases (FWD and RWD), the vehicle has been run on an aggressive driving scenario of modified WLTP cycle with 1.5 times the cycle speed and overall 7.5 times acceleration. Accelerator and brake pedal applications from the driver block have been limited for RWD to 94%, 83% and for FWD to 62%, 83% respectively. These limitation has been implemented following multiple acceleration and braking tests for restricting the wheels from entering into non-linear slip behaviour (see Figure 2) to avoid wheel lock-up or excessive spin up, thereby assuring the transmission of the highest possible demanded wheel force to the road (Figure 5).

Deceleration performance of both cases on this transient drive cycle is found to be very similar (Figure 5(B)) with matching driver brake pedal inputs (Figure 6(B)), meaning almost the same overall braking force is being put to the road. This shows that even if the powertrain has been placed in different locations (FWD and RWD), which affects the overall axle rotational inertia, the brake bias distribution and regenerative braking strategies hold the overall braking behaviour very close for the two cases. Acceleration to the desired speed for the RWD case is slightly compromised due to the limits of peak force transmission to the road (avoidance of rear-wheel spin up) due to restriction of torque demand to 94%. For the FWD case, the acceleration is much lower since the powertrain torque is restricted to 62% to avoid wheel spin (entering non-linear slip zone) and corresponding lower force transmission

(see Figure 2), which demonstrates the lower adhesion limits for FWD architecture when compared to RWD during acceleration.

**Figure 5** Comparison of: (A) Actual vehicle speed and (B) Acceleration rate for FWD and RWD in dynamic driving (see online version for colours)

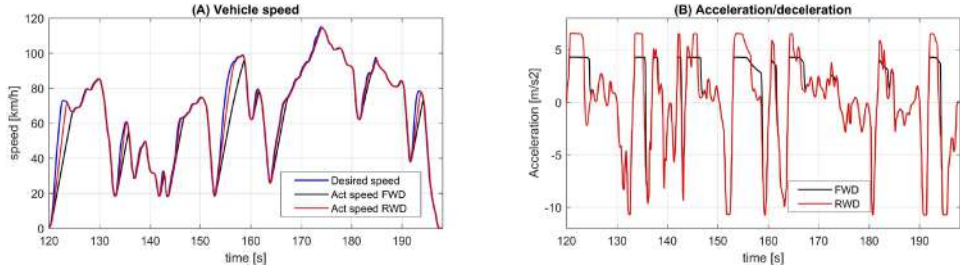
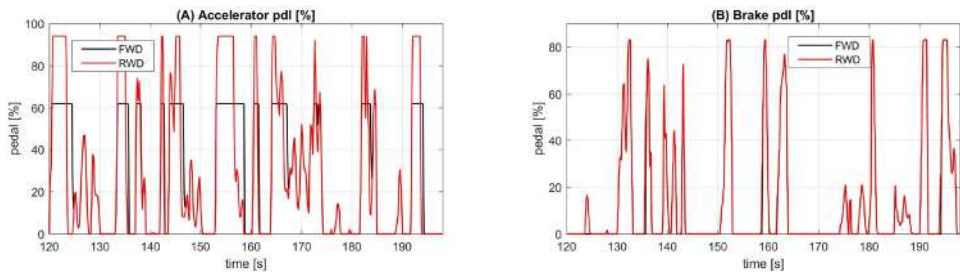
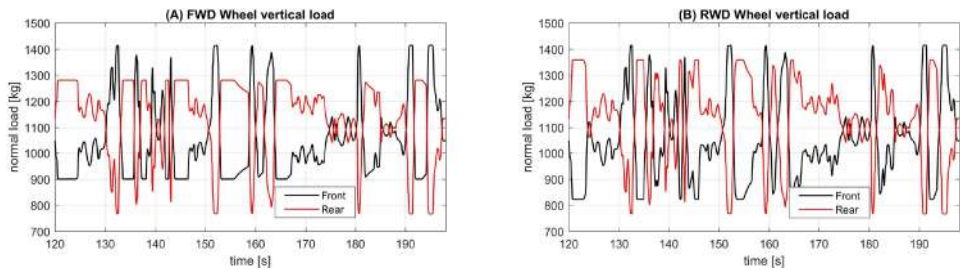


**Figure 6** Comparison of: (A) Accelerator pedal inputs and (B) brake pedal inputs for FWD and RWD in dynamic driving (see online version for colours)



As the vehicle accelerates we can see a decrease in normal load on the front axle and an increase on the rear axle, that is vertical load transfer from the front to the rear (Figure 7). In the case of deceleration, the opposite is evident. Load transfer from the front to the rear is much higher in the case of RWD as compared to FWD since the acceleration itself is higher. The magnitude of deceleration for both cases is similar and so is the normal load transfer from the rear to the front (Figure 7).

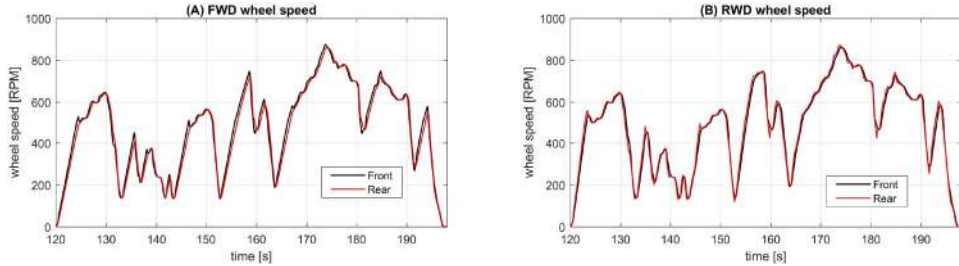
**Figure 7** Comparison of front and rear vertical wheel loads for: (A) FWD and (B) RWD cases in dynamic driving (see online version for colours)



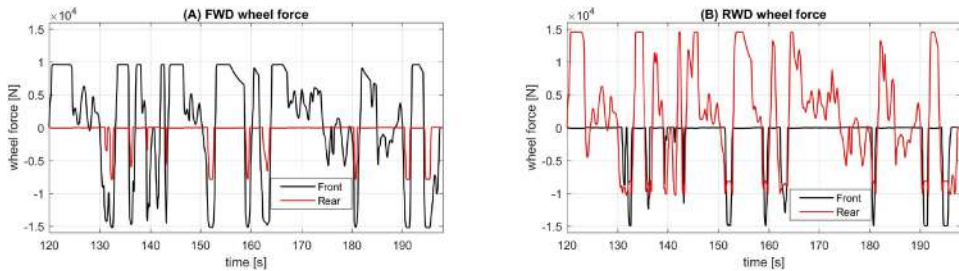
During acceleration, the speed of powered wheels for FWD and RWD show considerable positive speed difference as compared to driven wheels on accounts of positive slip

(Figure 8). During deceleration, the slip of powered wheels (front) for the FWD case is seen to be better controlled as compared to RWD due to its reduced adhesion limits in braking (normal load transfer)(Figure 7). Driven wheels for both cases show very similar speed profiles as that of the actual vehicle speeds (Figure 5), due to much lower wheel slips coming from almost zero force transmission during traction and low force transmission during braking (Figure 9).

**Figure 8** Comparison of front and rear actual wheel speeds for: (A) FWD and (B) RWD cases in dynamic driving (see online version for colours)



**Figure 9** Comparison of front and rear wheel transmitted force for: (A) FWD and (B) RWD cases in dynamic driving (see online version for colours)



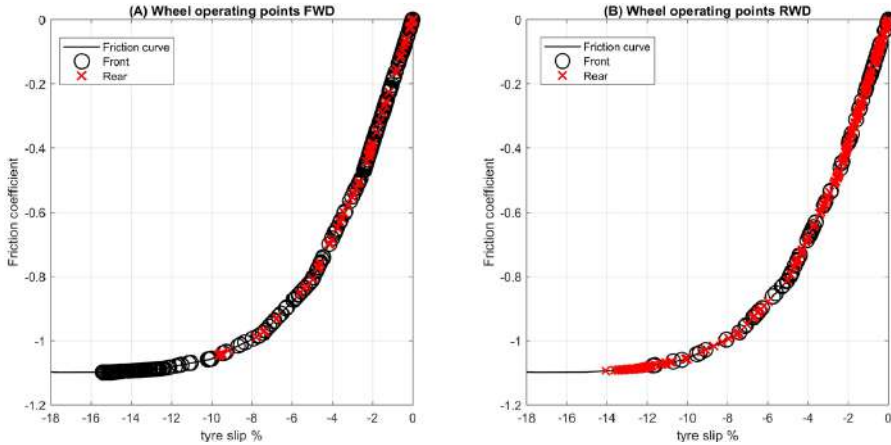
Tractive force from front wheels to the road in case of FWD is much constrained as compared to rear wheels for the RWD case (Figure 9) due to the limiting of driver accelerator inputs (Figure 6(A)). For both cases, the braking force is preferably transmitted by the powered wheels (Figure 9) with the application of a dedicated brake bias strategy to promote regenerative braking (refer to Figure 3, Figure 4). Support from the driven wheels in case of high deceleration demands is very evident for the RWD case due to the lower rear wheel adhesion limits and is less significant for FWD due to higher limits (effect of load transfer)(Figure 9).

Figure 10 shows slip-force behaviour of the powered and driven wheels for the FWD and RWD cases with regeneration focused braking strategies (refer to Figures 3 and 4).

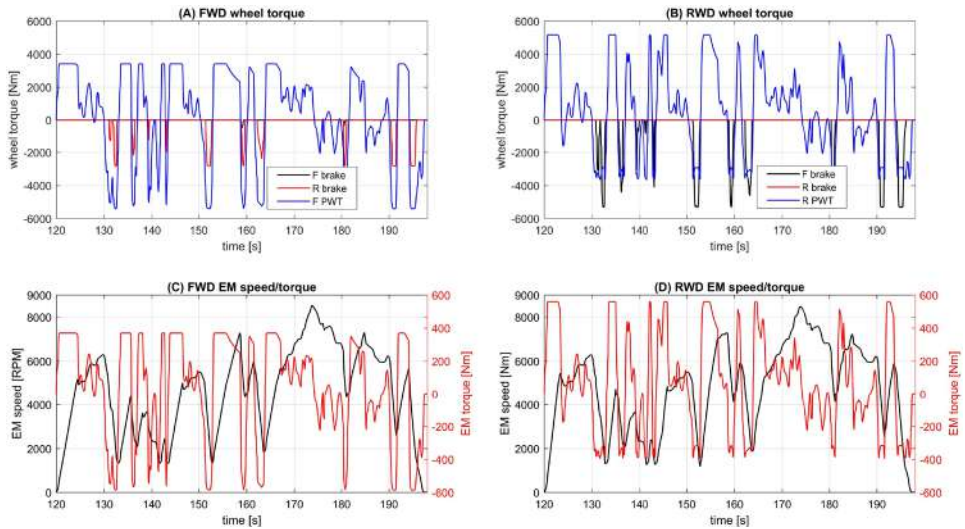
For the FWD case, the braking force is mostly transmitted by the front wheels (black) and is lightly supported by rear wheels (red) when the adhesion limits of the front are reached (Figure 10(A)). For the RWD case, the front wheel mechanical braking support is more prominent due to the lower ability of rear wheels to transmit braking force (Figure 10(B)).

Tractive wheel torque for the powered wheels (blue) of the FWD and RWD cases show the effect of limiting the driver accelerator demands to avoid wheel spin up (Figure 11(A) and (B)).

**Figure 10** Comparison of front and rear wheel operating points of slip-force relationship for: (A) FWD and (B) RWD cases in dynamic driving (see online version for colours)



**Figure 11** Comparison of wheel torque and EM torque, speed for FWD (A),(C) and RWD (B),(D) in dynamic driving (see online version for colours)



Comparing wheel braking torque for the two cases further shows lower support by the driven wheels (mechanical braking) to the powered wheels (blue) in the case of FWD as compared to RWD (Figure 11(A) and (B)). This is enforced by the brake bias distribution strategy to avoid rear wheel lock-up due to the much lower adhesion limit which is evident at higher brake pedal demands. At lower brake demands solely the powered wheels (blue) are capable of carrying out braking, maximising the recuperated energy.

At a few points for the FWD case (160 s, 180 s in (Figure 11(A))), we can also see some small front mechanical brake intervention to support the electrical powertrain braking as the limits of the EM regenerative torque are reached.

When comparing torque profiles for the front and rear (Figure 11) with the respective force transmission (Figure 9), we can see slightly different behaviour in terms of their

magnitudes due to the varying tyre slip-force relationship on accounts of normal load transfer (Figure 2). For the electric machine (EM) (Figure 11(C) and (D)), positive torque output to the powered wheels helps them turn, push the vehicle ahead and increase EM speed while negative torque output decreases the same. Due to a single gear reduction, EM speed for FWD and RWD cases follow the speed of their respective powered wheels (Figure 8). EM tractive torque for the FWD case is limited since the accelerator demand is highly constrained when comparing with the RWD case.

EM regenerative braking torque used for the RWD case is much lower as compared to the FWD case (Figure 11(C) and (D)) due to the difference in adhesion limits for front and rear wheels while braking. Apart from adhesion limited peak torque limits, the graph also shows the occurrence of torque restriction due to the EM power limit towards higher EM speeds (Figure 11). Positive EM and battery current represents traction (discharge) while negative represents energy recuperation in braking (charge) (Figure 12). The Tractive current for the FWD case is lower as compared to the RWD case due to restriction in its tractive performance on accounts of wheel adhesion limits. Similarly, the regenerative current is higher for the FWD case as compared to the RWD case due to its higher adhesion limits in braking.

**Figure 12** Comparison of EM and battery current for: (A) FWD and (B) RWD in dynamic driving (see online version for colours)

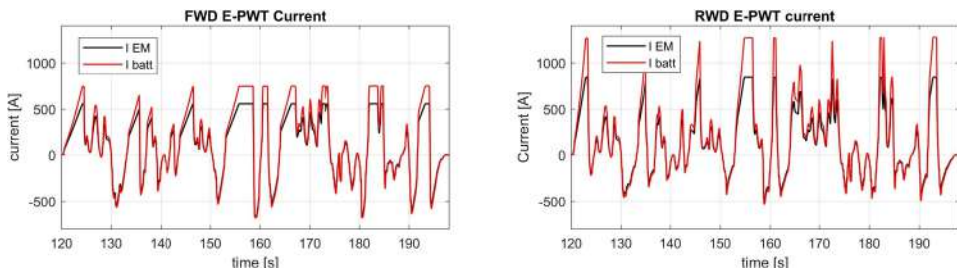


Figure 13 represents battery actual and open-circuit voltages. Fall in actual battery voltage and open-circuit voltage signifies battery discharging whereas, a rise shows charging. A higher soar of actual battery voltage for the FWD as compared to the RWD case represents higher regenerative braking power (charging). A greater drop in the actual battery voltage of RWD as compared to the FWD case is due to the higher battery discharge from greater acceleration. Finally, the consequence of lower regenerative braking and higher tractive discharge for RWD as compared to the FWD case leads to a greater fall in its battery State of Charge *SoC* over the complete driving cycle (Figure 14).

## 5.2 200-0 braking test

This high-speed braking test has been used to further analyse the effect of the electrical powertrain placement (FWD or RWD) and corresponding wheel-vehicle dynamics on energy recuperation through regenerative braking. For an increasing brake pedal application on the 200-0 km/h braking test, the deceleration at 100km/h instant tends to increase proportionally and at almost the same rate for both front and rear regeneration focused FWD and RWD cases (Figure 15(A)). The 200-0 km/h stopping distance initially drops heavily followed by a gradual decrease as with higher brake input the vehicle simply spends lesser time at greater speeds and thus covers lesser distance before stopping (Figure 15(B)).

In addition, the wheel slip, braking torque, braking road force and vertical load transfer have been presented (see Figure 16). Until 35% pedal application for the 100 km/h instant, the braking force from the powered wheels to the road rises proportionally with the application of increasing regenerative braking torque (blue) (Figure 16(C) and (D)). This increase in braking force comes from the generated negative wheel slip (Figure 16(A)) (refer to Figure 2).

**Figure 13** Comparison of actual and open circuit battery voltage for: (A) FWD and (B) RWD in dynamic driving (see online version for colours)

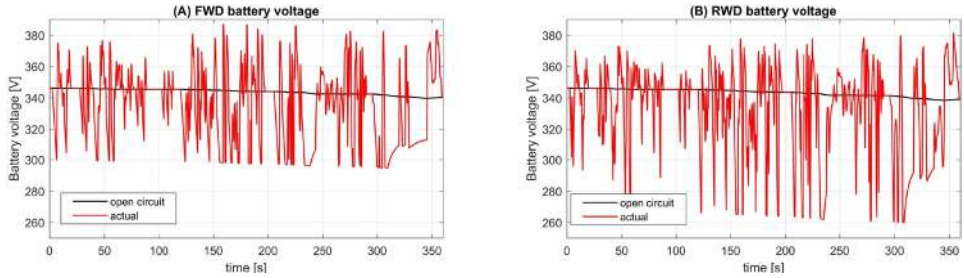
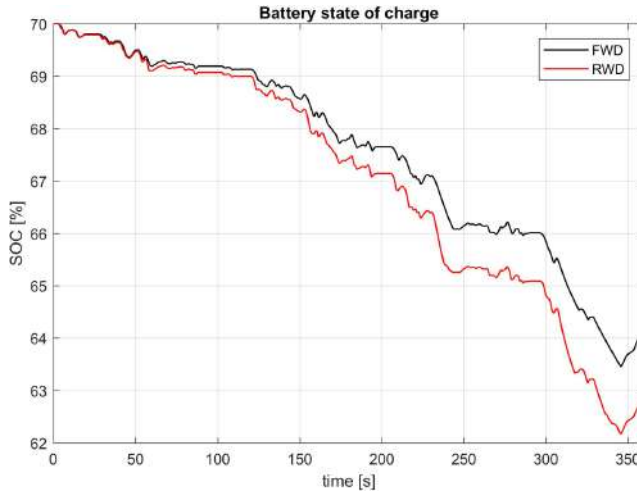


**Figure 14** Comparison of battery SoC for FWD and RWD architectures in dynamic driving (see online version for colours)



The normal vertical load transfer from rear to front depends on the deceleration and thus rises proportionally with increasing brake pedal demand (Figure 16(B)). With higher load transfer, the limits of adhesion for rear wheels of the RWD case get tested earlier at around 35% (red–), and to avoid their lock-up front wheel braking is introduced to assist in deceleration (black–) (Figure 16(D)). For the FWD case, a similar effect is seen much later at around 45% demand (black) (due to normal load transfer from rear to front) when the grip of the front powered wheels is no longer solely enough to fulfil the required braking performance.

On further increase in brake pedal demand for RWD case above 35% after the introduction of mechanical braking on the front dead axle (black–) (Figure 16(D)), the transmitted force

**Figure 15** Comparison of: (A) deceleration rate and (B) braking distance at 100 km/h for 200-0 braking test

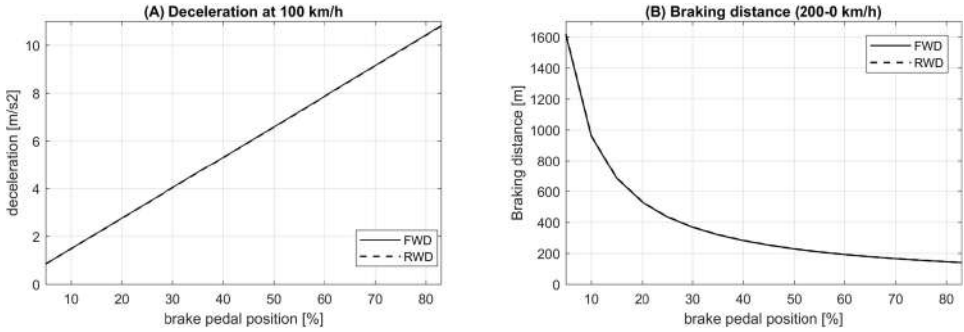
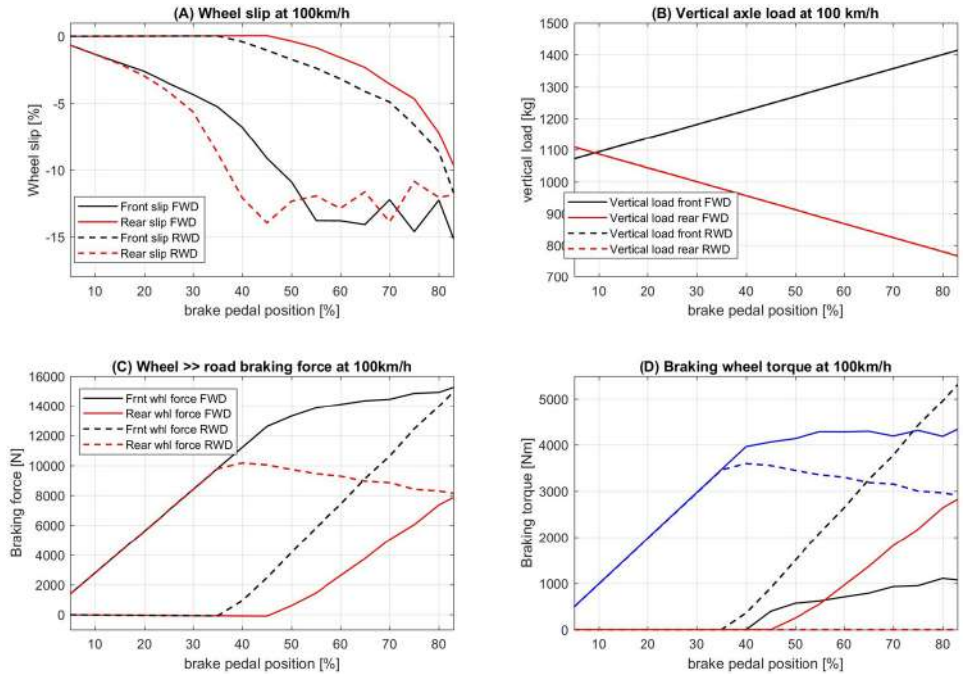


**Figure 16** Comparison of: (A) wheel slip; (B) vertical load; (C) braking force and (D) wheel torque at 100km/h for 200-0 braking test (see online version for colours)



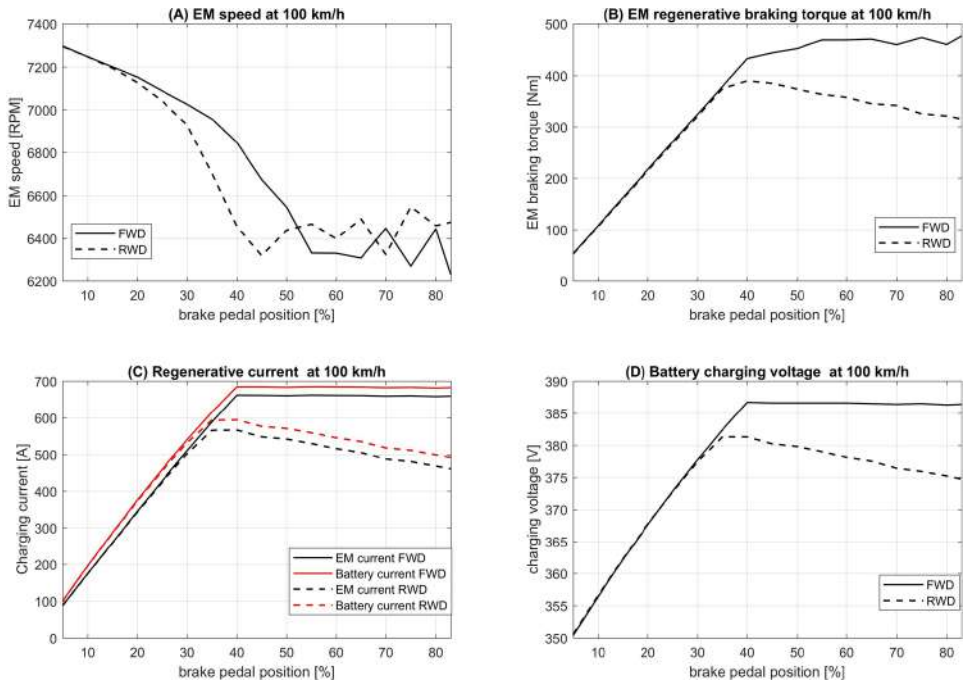
from the rear (powered wheels) is further decreased (red-) to avoid lock-up due to the decreasing vertical load on the rear for increasing deceleration (Figure 16(C)). On the other hand, at this level of pedal application, the transmitted force for front wheels of the FWD case continues to rise (black) even after the introduction of rear brakes due to their increasing adhesion limits with a greater normal load on the front (Figure 16(C)). With the introduction of mechanical braking for the dead axles, their tyre slip also increases and so does their transmitted braking force for both cases (Figure 16(A) and (C)). A higher rise in the negative slip of powered wheels for RWD as compared to FWD from 0–35% pedal input further shows the lower ability of the rear wheels to transmit braking force for a certain level of

wheel slip (due to load transfer), requiring more slip to generate the same amount of braking force.

For the powered rear wheels of the RWD case, mechanical braking torque is never seen to be introduced at 100 km/h instant as the rear torque demand for all brake pedal inputs can be met solely by the electric machine (blue –)(Figure 16(D)). This differs in the case of FWD where for the 100 km/h instant, the EM torque (blue) is not solely sufficient at higher pedal demands (>40%) due to greater force/torque transmission capability and thus has to be supported by mechanical brakes (black). At peak braking demand (83%), the rear wheel braking torque for both FWD (red) and RWD (blue–) reach almost the same value whereas when comparing for the front wheels of both cases, the mechanical torque for RWD case (black–) and the sum of regenerative and supplementary front mechanical torque for FWD case (blue and black) seem to hold a similar value (Figure 16(D)).

With an increase in the brake pedal demand, the EM speed decreases to lower values and holds around 6400 RPM (Figure 17(A)) due to the similar level of negative slip of the powered wheels for both FWD and RWD cases at the 100 km/h instant (see Figure 16(A)).

**Figure 17** Comparison of: (A) EM speed; (B) EM braking torque; (C) battery current and (D) voltage at 100 km/h for 200-0 braking test (see online version for colours)

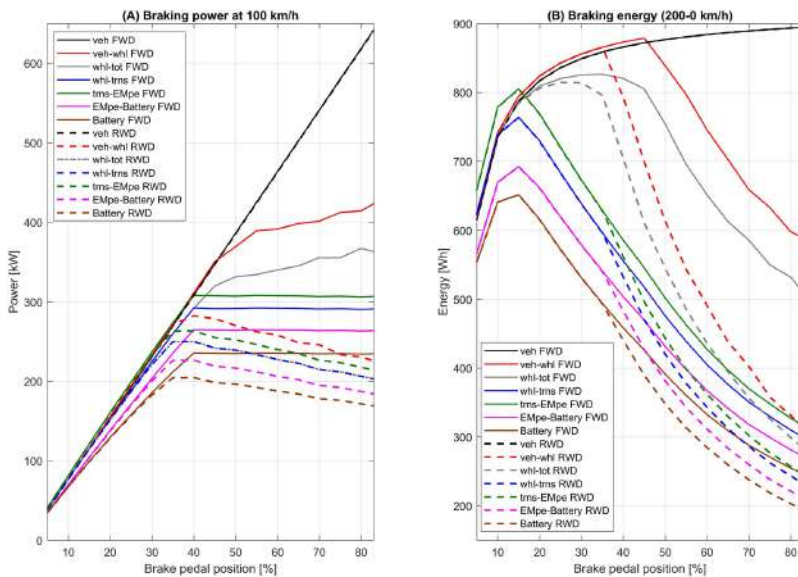


At these speeds, the EM is easily capable of supplying for any rear-wheel torque demand (RWD case)(see Figure 4) but not for increasing levels of front-wheel torque demands (FWD case) which is evident from the introduction of mechanical braking to the powered wheels (see Figure 16). The EM regenerative torque for the FWD case reaches around 450 Nm and remains unchanged after due to EM power limitation (refer to Figure 4(B)). For the RWD case, the EM torque above 35% is not decreasing due to the EM torque limits but on accounts of the changing brake bias strategy for avoiding rear wheel lock-up. Maintaining

high regenerative braking torque for the FWD case on increasing pedal demands results in higher charging current and charging voltage to the battery whereas, for the RWD case, the peak of charging current and battery voltage is reached at peak regenerative torque after which they gradually drop due to rear wheel adhesion limits (Figure 17(C) and(D)).

Considering braking power and braking energy analysis for the 200-0 km/h braking test (Figure 18), the braking power requirement at the 100 km/h instant for the complete vehicle (black) is directly proportional to the deceleration and thus also to the increasing pedal demand (Figure 18(A)). Overall vehicle braking energy for the 200-0 braking test (black) (Figure 18(B)) initially rises quickly and then slowly with increasing pedal application, as with increasing deceleration the vehicle spends lesser time at high speeds and the overall energy loss to aerodynamic drag and other vehicle resistances decreases, increasing the actual vehicle braking energy from the braking system.

**Figure 18** Comparison of: (A) braking power at 100 km/h and (B) braking energy on 200-0 braking test for range of brake pedal inputs (see online version for colours)



Until 35% demand for RWD and 45% for FWD cases, slightly more braking power is given by the powered wheels to the road (red) than the overall vehicle body stopping power (black) to also counter the resistance from the deceleration of the driven non-powered wheels rotating inertias (Figure 18(A)). This is more evident from the difference in the braking energy at vehicle body (black) and that transmitted between the powered wheels and road for the complete event (red) (Figure 18(B)). At higher brake pedal demands (above 40%) the difference in braking power, energy transmitted between powered wheels and road interface (red) and that required to stop the vehicle (black) is coming from the mechanical braking support of the other non powered wheels due to adhesion limitations of the powered wheels and the avoidance of their lock-up by the previously discussed brake bias strategies.

For both cases, the difference in braking power and energy transmitted at the wheel-road interface (red) and the total efforts (braking torque) to the powered wheels (grey) is on accounts of wheel slip losses. For minor braking force transmission, the corresponding slip

rises almost proportionally while at elevated pedal inputs with higher force transmission requirement, the wheel slip has to increase drastically making its losses significant above 15% demand (Figure 2). For both cases, the effect of powered wheel inertias will act to reduce this difference by increasing the powertrain regeneration due to their resistance to slowing down and stored energy.

The deviation in the total braking efforts to the powered wheels (grey) and those from the electrical powertrain (blue) comes from the losses to the supporting mechanical brakes on the powered axle. For RWD this power loss is absent for all pedal demands as the electrical powertrain is solely capable of providing the necessary braking torque at the 100 km/h instant for the complete range of brake pedal applications. For FWD case above 40% demand, we see a gradually increasing intervention of mechanical brakes as the adhesion levels of the front powered wheels increase (grey) and surpass the limited braking capability of the electrical powertrain (blue) due to which the regeneration power for the FWD case at various powertrain levels also gets curtailed (green, pink, brown).

On comparison of the energy flow for the 200-0 km/h complete braking event (Figure 18(B)) we see the whole picture where the support from mechanical brakes (at powered wheels) is evident even for the RWD case which is not evident at the 100 km/h instant. The FWD mechanical brakes intervention on the powered wheels remains much higher than RWD above 35% throughout the range of pedal applications as the decreasing adhesion for the RWD case starts affecting the system. Above 35% the powertrain braking power and energy for RWD (blue-) also decreases as compared to FWD (blue) for the same reason of declining rear wheel adhesion and the corresponding effect of brake bias strategy in reducing the braking torque to avoid lock-up.

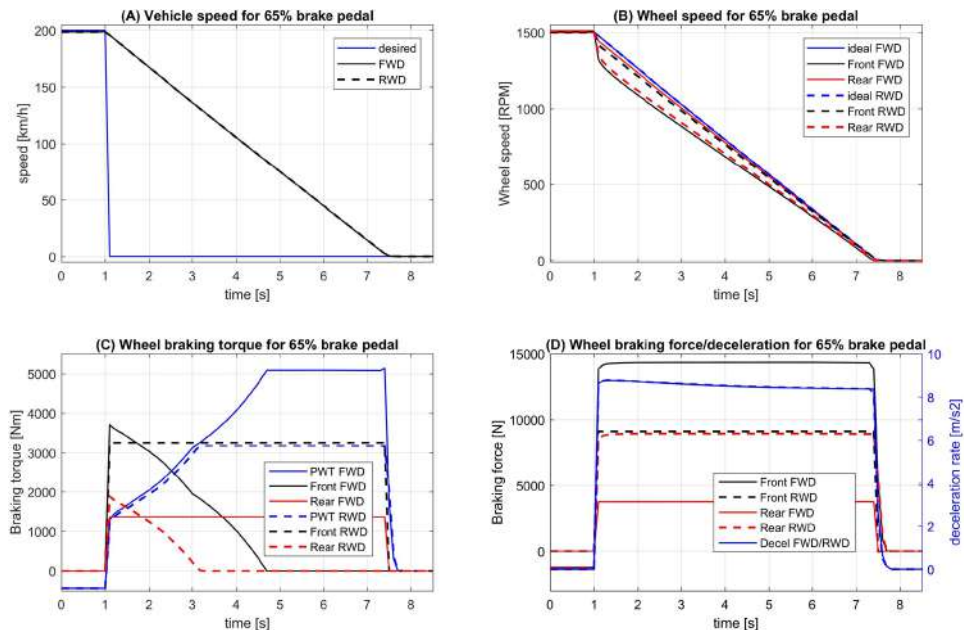
The power/energy flow between the electric machine and transmission (green) is greater than that between the transmission – wheel (blue) as although there is an impact of the frictional losses in the transmission (5%), the energy stored in rotational inertia of the complete traction chain and the corresponding resistance to its slow down more than compensates for the frictional losses. The difference between EM – power electronics (pink) and EM – transmission (green) is due to the fixed electrical losses in the electric drive. The decrease in final stored battery power, energy (brown) over that coming from the EM – PE interface (pink) is purely due to the internal losses of the battery module.

Considering the peaks of regenerative energy at various traction chain levels (Figure 18(B)), the faster the vehicle body stops, the more will be the vehicle body braking energy (black). The highest limit of powered wheel to road energy transmission (red) comes in the middle of braking demand as a result of introducing braking by the non powered wheels for the avoidance of powered wheel lock-up (FWD – 45%, RWD – 35%). The highest recoverable energy from the powered wheels (grey) is around 20-40% instead of 30-50% pedal demand on accounts of elevated wheel slip losses with increasing brake pedal application. The peak of actual recuperated energy from the powered wheels (blue) is at lower brake pedal demand (15%) than expected (20–45%) due to the support from mechanical brakes (electrical powertrain torque limitation).

To further analyse the interaction of mechanical and electrical braking over the complete 200-0 km/h braking event, we now compare the FWD and RWD cases for 65% pedal application wherein with very similar deceleration rates, the vehicle speeds for both FWD and RWD cases drop in the same manner and the vehicles stop at almost the same point (see Figure 19(A)). The total wheel force to the road in both cases remains almost the same throughout the braking event (see Figure 19(D)). The wheel-braking force from the FWD front wheels is much higher than from the FWD rear wheels to promote regenerative braking

while also maintaining the demanded high deceleration performance. Braking wheel Forces for RWD case from the front and rear wheels are very similar for 65% pedal application to again maintain the highest possible rear braking for maximising energy recuperation while avoiding rear wheel lock-up (Figure 19(D)). Front wheels for the FWD case show the highest drop in wheel speed (negative slip) as they transmit the highest amount of wheel force while the opposite is seen for the FWD rear wheels (see Figure 19(B)). For the RWD case, although both front and rear wheels transmit almost the same level of braking force to the road (see Figure 19(D)), the RWD rear powered wheel slip is a lot higher than the RWD front wheel slip due to the decreasing adhesion on the rear on accounts of normal load transfer from the rear to the front (see Figure 19(B)). Braking torque to the powered wheels for both cases now shows clear presence of mechanical braking assistance at higher vehicle speeds as the powertrains are restricted by lower electric drive torque limits (see Figure 19(C)). As the vehicle speed drops, so does the speed of the electric machine and its peak torque level rises. Since the braking torque demand for RWD rear wheels is lower (to avoid lock-up due to lower adhesion) the powertrain can completely take over the braking event much earlier as compared to the FWD front wheels where braking torque demand is much higher (see Figure 19(C)).

**Figure 19** Comparison of: (A) vehicle speed; (B) wheel speed; (C) braking torque and (D) braking force and deceleration rate on 200-0 braking test for 65% pedal demand (see online version for colours)



## 6 Conclusions and perspectives

In this paper, feed-forward brake bias distribution strategies for front wheel drive (FWD) and rear wheel drive (RWD) electric powertrains favouring the usage of the powered wheels to

maximise the regenerative braking have been implemented and analysed. First, the selected modelling methodologies for vehicle dynamics and all relevant components of the traction chain have been presented. For investigating the effect of the proposed braking strategies on energy recuperation as well as drivability, especially under intense driving situations, various simulation results have been discussed.

The results for a high-speed driving scenario with pronounced impact of the front, rear wheel slip and normal load transfer have been used to compare the effect of the proposed regenerative braking and brake bias strategies for the two powertrain placement cases (FWD and RWD). Here, the focus has been on an overall system analysis including the effect of heavy braking as well as rapid accelerations on the corresponding vehicle and powertrain dynamics, efficiency and stability.

For a detailed analysis of the impact of pronounced vehicle dynamics on regenerative braking of FWD and RWD cases, a 200-0 km/h braking test has been considered. As expected, at lower brake pedal demands, both FWD and RWD regeneration focused cases show similar energy recuperation potential, powertrain and vehicle dynamics behaviours. When braking aggressively at higher vehicle speeds, the regeneration potential of the RWD case is primarily limited by the decreasing powered wheel adhesion limits due to the vertical load transfer from the rear to the front of the vehicle. For the FWD case, this adhesion limit rises with higher deceleration and here the regeneration gets constrained by the peak torque limit of the electric machine. After the peak of regeneration for the high speed braking test at around 15% brake pedal demand, the recuperated energy at different levels in the traction chain drops due to various limitations and losses associated with wheel adhesion limits (avoiding lock-up), powertrain torque capacities and increasing tyre slip.

To sustain efficient regenerative braking characteristics at even higher brake pedal applications and vehicle speeds, innovative strategies which manage powered wheel slip by transferring the braking responsibilities to the driven wheels could be further explored.

## Acknowledgement

The Altran Prototype Automobile (APA group), Research & Innovation Department, Capgemini Engineering, supported this work, under the project Hybrid Innovative Powertrain (HIP). The authors would like to thank the other members of the team Guillaume Voizard, Michel Geahel, Frédéric Guimard, Adrien Chamero and Kamal Nouri.

## References

- Ahmadi, S., Bathaee, S. and Hosseinpour, A.H. (2018) 'Improving fuel economy and performance of a fuel-cell hybrid electric vehicle (fuel-cell, battery, and ultra-capacitor) using optimized energy management strategy', *Energy Conversion and Management*, Vol. 60, pp.74–84.
- Bruen, T. and Marco, J. (2016) 'Modelling and experimental evaluation of parallel connected lithium ion cells for an electric vehicle battery system', *Journal of Power Sources*, Vol. 310, pp.91–101.
- Clegg, S.J. (1996) *A Review of Regenerative Braking Systems*, Institute of Transport Studies.
- Crolla, D. and Cao, D. (2012) 'The impact of hybrid and electric powertrains on vehicle dynamics, control systems and energy regeneration', *Vehicle System Dynamics*, Vol. 50, sup1, pp.95–109.
- D.Sherman (2014) *Five Slippery Cars Enter a Wind Tunnel, One Slinks Out A Winner, comparo*.

- Du, J., Chen, J., Song, Z., Gao, M. and Ouyang, M. (2017) 'Design method of a power management strategy for variable battery capacities range-extended electric vehicles to improve energy efficiency and cost-effectiveness', *Energy*, Vol. 21, pp.32–42.
- Ehsani, M., Gao, Y., Longo, S. and Ebrahimi, K. (2018) *Modern Electric, Hybrid Electric, and Fuel Cell Vehicles, Third Edition*, CRC Press, DOI:<https://doi.org/10.1201/9780429504884>.
- EU (2016) *European Commission. A European Strategy for Low-Emission Mobility*.
- Guo, H., Zhang, J., Geng, W., Cheng, H. and Yu, H. (2021) 'Research on regenerative braking strategies for hybrid electric vehicle by co-simulation model', *International Journal of Vehicle Performance (IJVP)*, Vol. 7, Nos. 3–4, pp.1461–1477.
- Guo, J., Wang, J. and Cao, B. (2009) 'Regenerative braking strategy for electric vehicles', *2009 IEEE Intelligent Vehicles Symposium*, IEEE, pp.864–868, DOI:10.1109/IVS.2009.5164393.
- Guzzella, L. and Sciarretta, A. (2013) *Vehicle Propulsion Systems*, Springer Berlin Heidelberg.
- He, R., Zheng, H. and Zong, C. (2014) *Braking Force Distribution and Coordinated Control Algorithm for Hybrid Electric Bus based on EBS*, DOI:<https://doi.org/10.4271/2014-01-1908>
- Henaio-Muñoz, A.C., Pereirinha, P. and Bouscayrol, A. (2020) 'Regenerative braking strategy of a formula SAE electric race car using energetic macroscopic representation', *World Electric Vehicle Journal*, Vol. 1, No. 2, p.45.
- Hofman, T., Steinbuch, M., van Druten, R. and Serrarens, A. (2006) 'Rule-based energy management strategies for hybrid vehicle drivetrains: a fundamental approach in reducing computation time', *IFAC Proceedings Volumes*, Vol. 39, No. 16, pp.740–745.
- Hust, F.E. (2018) *Physikalisch-chemisch motivierte Parametrierung und Modellierung von echtzeitfähigen Lithium-Ionen Batteriemodellen - eine Fallstudie zur Tesla Model S Batterie*, PhD thesis.
- IEA (2018) *Towards Cross-Modal Electrification*, IEA. Global EV.
- Itani, K., De Bernardinis, A., Khatir, Z. and Jammal, A. (2016) 'Comparison between two braking control methods integrating energy recovery for a two-wheel front driven electric vehicle', *Energy Conversion and Management*, Vol. 22, pp.330–343.
- Jacobson, B. (2016) *Vehicle Dynamics Compendium, Vehicle Dynamics Group, Division of Vehicle and Autonomous Systems*, Department of Applied Mechanics, Chalmers University of Technology.
- James, S.S., Anderson, S.R. and Lio, M.D. (2020) 'Longitudinal vehicle dynamics: a comparison of physical and data-driven models under large-scale real-world driving conditions', *IEEE Access*, Vol. 8, pp.73714–73729.
- Jiang, X., Chen, L., Xu, X., Cai, Y., Li, Y. and Wang, W. (2018) 'Analysis and optimization of energy efficiency for an electric vehicle with four independent drive in-wheel motors', *Advances in Mechanical Engineering*, Vol. 10, No. 3, 168781401876554, DOI:<https://doi.dox.org/10.1177/1687814018765549>
- Kuhlwein, J. (2016) *Driving Resistances of Light-Duty Vehicles in Europe: Present Situation, Trends, and Scenarios for 2025*, The International Council on Clean Transportation.
- Kumar, N. and Subramanian, S. (2015) 'Cooperative control of regenerative braking and friction braking for a hybrid electric vehicle', *Proceedings of the Institution of Mechanical Engineers, Part D: Journal of Automobile Engineering*, Vol. 230, No. 1, pp.103–116.
- Le Sollicec, G., Chasse, A. and Geamanu, M. (2013) 'Regenerative braking optimization and wheel slip control for a vehicle with in-wheel motors', *IFAC Proceedings Volumes*, Vol. 46, No. 21, pp.542–547, 7th IFAC Symposium on Advances in Automotive Control.
- Niestadt and Bjørnåvold (2019) *Electric Road Vehicles in the European Union-Trends, Impacts and Policies*, European Parliamentary Research Service (EPRS).
- Oleksowicz, S., Burnham, K., Southgate, A., McCoy, C., Waite, G., Hardwick, G., Harrington, C. and McMurran, R. (2013) 'Regenerative braking strategies, vehicle safety and stability control systems: Critical use-case proposals', *Vehicle System Dynamics*, pp.1–16.

- Pacejka, H.B. (2000) 'Modelling of tyre force and moment generation', *Rolling Contact Phenomena*, Springer Vienna, pp.277–327.
- Pardhi, S. (2020) 'Simulation and analysis of 48v mild hybrid, CVT, and upcoming powertrain control strategies for increasing light vehicle fuel efficiency', *International Journal of Engineering Research and Technology*, Vol. 9, pp.620–634.
- Pardhi, S., Deshmukh, A. and Ajrouche, H. (2021) 'Modelling and simulation of detailed vehicle dynamics for the development of innovative powertrains', *International Journal of Automotive Sc and Technology*, Vol. 5, pp.244–253.
- Qiu, C., Wang, G., Meng, M. and Shen, Y. (2018) 'A novel control strategy of regenerative braking system for electric vehicles under safety critical driving situations', *Energy*, Vol. 49, pp.329–340.
- Rabhi, A., M'Sirdi, N. and Elhajjaji, A. (2007) 'Estimation of contact forces and tire road friction', *2007 Mediterranean Conference on Control and Automation*, IEEE, pp.1–6, DOI:10.1109/MED.2007.4433875.
- Ruan, J., Zhu, B. and Walker, P. (2014) *Experimental Verification of Regenerative Braking Energy Recovery System based on Electric Vehicle Equipped with 2-Speed DCT*, pp.1–8, DOI: 10.1049/cp.2014.0356.
- Sangtarash, F., Esfahanian, V., Nehzati, H., Haddadi, S., Bavanpour, M.A. and Haghpanah, B. (2008) 'Effect of different regenerative braking strategies on braking performance and fuel economy in a hybrid electric bus employing CRUISE vehicle simulation', *SAE International Journal of Fuels and Lubricants*, No. 1, pp.828–837.
- Shakouri, P., Laila, D., Ordys, A. and Askari, M. (2010) *Longitudinal Vehicle Dynamics using Simulink/Matlab*, DOI:10.1049/ic.2010.0410.
- Singh, K.B. and Taheri, S. (2014) 'Estimation of tire–road friction coefficient and its application in chassis control systems', *Systems Science and Control Engineering*, Vol. 3, No. 1, pp.39–61.
- Tesla (2012) Tesla.com, Tesla.
- Wang, F. and Zhuo, B. (2008) 'Regenerative braking strategy for hybrid electric vehicles based on regenerative torque optimization control', *Proceedings of the Institution of Mechanical Engineers, Part D: Journal of Automobile Engineering*, Vol. 222, No. 4, pp.499–513.
- Xiao, B., Lu, H., Wang, H., Ruan, J. and Zhang, N. (2017) 'Enhanced regenerative braking strategies for electric vehicles: Dynamic performance and potential analysis', *Energies*, Vol. 10, No. 11, p.1875, DOI:https://doi.org/10.3390/en10111875
- Xu, G., Li, W., Xu, K. and Song, Z. (2011) 'An intelligent regenerative braking strategy for electric vehicles', *Energies*, Vol. 4, No. 9, pp.1461–1477.
- Xu, W., Chen, H., Zhao, H. and Ren, B. (2019) 'Torque optimization control for electric vehicles with four in-wheel motors equipped with regenerative braking system', *Mechatronics*, Vol. 57, pp.95–108.
- Zhang, J., Lv, C., Gou, J. and Kong, D. (2012) 'Cooperative control of regenerative braking and hydraulic braking of an electrified passenger car', *Proceedings of the Institution of Mechanical Engineers, Part D: Journal of Automobile Engineering*, Vol. 226, No. 10, pp.1289–1302.